

Exciton-phonon interactions in nanocavity-integrated monolayer transition metal dichalcogenides

David Rosser¹, Taylor Fryett², Albert Ryou², Abhi Saxena², and Arka Majumdar^{1,2,*}

¹Department of Physics, University of Washington, Seattle, Washington 98195, USA

²Department of Electrical and Computer Engineering, University of Washington, Seattle, Washington 98195, USA

*Corresponding Author: arka@uw.edu

February 18, 2022

Abstract

Cavity-integrated transition metal dichalcogenide excitons have recently emerged as a promising platform to study strong light-matter interactions and related cavity quantum electrodynamics phenomena. While this exciton-cavity system is typically modeled as coupled harmonic oscillators, to account for the rich solid-state environment the effect of exciton-phonon interaction needs to be incorporated. We model the system by including a phenomenological deformation potential for exciton-phonon interactions and we elucidate the experimentally measured preferential coupling of the excitonic photoluminescence to the cavity modes red-detuned with respect to the exciton resonance. Furthermore, we predict and experimentally confirm the temperature dependence of this preferential coupling. By accurately capturing the exciton-phonon interaction, our model illuminates the potential of cavity-integrated transition metal dichalcogenides for development of low-power classical and quantum technologies.

1 Introduction

Atomically thin van der Waals materials have recently emerged as a promising platform for engineering novel light-matter interactions [1, 2, 3]. Among various van der Waals materials, the semiconducting transition metal dichalcogenides (TMDCs) allow for the robust exploration of cavity quantum electrodynamics

(cQED) in an ostensibly scalable system by their direct integration with on-chip, planar nanophotonic cavities [3, 4]. In this hybrid system, the TMDC excitons evanescently couple to the photonic modes. Several recent studies have reported cavity integration of these materials exhibiting optically pumped lasing [5, 6, 7, 8], cavity enhanced second harmonic generation [9, 10], cavity enhanced electroluminescence [11], and strong coupling [12]. Beyond these demonstrations, there exist theoretical proposals utilizing TMDC excitons for quantum optical applications in single photon non-linear optics [13, 14].

A necessary step for elucidating the potential applications of cavity-integrated TMDCs is an understanding of the relevant underlying physics of the exciton-cavity interaction. The prevailing description of the interaction between TMDC excitons and quantum optical cavity modes largely neglects the role of the solid state environment. However, exciton-phonon interactions are known to have a significant effect on the neutral exciton photoluminescence (PL) [15, 16, 17, 18, 19, 20, 21]. In other solid-state cQED systems, such as self-assembled quantum dots coupled to nanocavities, the exciton-phonon interaction is known to cause an asymmetric photoluminescent lineshape in the form of phonon sidebands, as well as modify the cavity-coupled photoluminescence [22, 23, 24]. In addition, after a careful review of the published literature on TMDCs coupled to whispering gallery mode resonators, we find multiple instances where the exciton's photoluminescence emission into the cavity modes appear preferentially coupled to the red-detuned side of the exciton resonance [6, 7, 25, 26]. This intriguing asymmetric coupling between the excitons and the cavity modes, which is not predicted by the simple coupled oscillator exciton-cavity theory, points to an important missing parameter in the model.

In this paper we investigate the role of phonons in the coupling of monolayer TMDCs to nanophotonic resonators. Coupling of the TMDC neutral exciton to a cavity mode is represented as coupled oscillators within the rotating wave approximation [14, 27] and a deformation potential is used to model the exciton-phonon interaction [28, 29], similar to the studies in self-assembled quantum dots coupled to nanocavities. An effective master equation is employed to describe phonon-mediated decay processes and incoherent exciton-cavity coupling [30]. Experimentally, we placed monolayer WSe₂ onto a silicon nitride ring resonator which allows for the simultaneous measurement of multiple cavity modes at different detunings. Our model exhibits preferential coupling of the exciton emission to red-detuned cavity modes, faithfully reproducing the experimental data. We further validate the theoretical model with a prediction and experimental confirmation that the asymmetry decreases with increasing temperature.

2 Polaron Master Equation

A homogenous distribution of TMDC excitons and a single, dispersionless cavity mode is typically formulated in terms of a coupled oscillator model H_{XC} wherein the exciton and cavity coherently interact via an exciton-cavity coupling g [14, 27]. The resonance frequency can be measured with respect to a rotating frame

at the resonant drive frequency ω_L . The deformation potential exciton-phonon interaction H_{XP} [28, 29] is similar to that seen in the spin-boson model [31, 32] or for optomechanical systems [33] where the exciton number operator is coupled to a bath of harmonic oscillators b_q with frequency ω_q and coupling λ_q . Thus the coupled system is described by the Hamiltonian $H = H_{XC} + H_{XP}$

$$\begin{aligned} H_{XC} &= \hbar\Delta_{XL}a^\dagger a + \hbar\Delta_{CL}c^\dagger c + \hbar g(a^\dagger c + c^\dagger a) \\ H_{XP} &= \hbar a^\dagger a \sum_q \lambda_q (b_q + b_q^\dagger) + \sum_q \hbar\omega_q b_q^\dagger b_q \end{aligned}$$

where $\Delta_{XL} = \omega_X - \omega_L$ and $\Delta_{CL} = \omega_C - \omega_L$ are the detunings of the exciton and the cavity from the laser wavelength, respectively; a (c) is the annihilation operator for the exciton (cavity) mode. In the weak excitation regime we neglect exciton saturation and any exciton-exciton interaction. Hence, we can treat both exciton and cavity operators as bosonic.

In order to distinguish the observed neutral exciton from the effects associated with phonon bath induced fluctuations, we use the polaron transformation $P = a^\dagger a \sum_q \frac{\lambda_q}{\omega_q} (b_q^\dagger - b_q)$ with $H \rightarrow e^P H e^{-P}$ [34], which leads to the system Hamiltonian (Supplementary Materials) [31, 33, 35, 36]

$$H'_S = \hbar(\Delta_{XL} - \Delta_P)a^\dagger a - \hbar\Delta_P a^\dagger a^\dagger a a + \hbar\Delta_{CL}c^\dagger c + \hbar\langle B \rangle g(\sigma^+ a + a^\dagger \sigma^-) \quad (1)$$

The exciton resonance $\Delta'_{xL} = \Delta_{xL} - \Delta_P$ is renormalized by a polaron shift $\Delta_P = \sum_q \frac{\lambda_q^2}{\omega_q}$, which is analogous to a Lamb shift [37]. When the harmonic oscillator bath is written in terms of the phonon displacement operator $B_\pm = \exp[\pm \sum_q \frac{\lambda_q}{\omega_q} (b_q - b_q^\dagger)]$ the exciton-cavity coupling is modified from the bare value by the average phonon displacement $\langle B \rangle$

$$\langle B \rangle = \exp\left[-\frac{1}{2} \sum_q \left(\frac{\lambda_q}{\omega_q}\right)^2 (2\bar{n}_q + 1)\right]$$

where $\bar{n}_q = [e^{\beta\hbar\omega_q} - 1]^{-1}$ is the mean phonon number with bath temperature $T = 1/k_B\beta$ [38]. As the temperature increases, the average phonon number in each mode increases, which decreases the exciton-cavity interaction.

We employ an effective master equation $\frac{\partial\rho}{\partial t} = \frac{1}{i\hbar}[H', \rho] + \frac{\kappa}{2}\mathcal{L}[c] + \frac{\gamma}{2}\mathcal{L}[a] + \frac{\Gamma_{ph}^{a^\dagger c}}{2}\mathcal{L}[a^\dagger c] + \frac{\Gamma_{ph}^{c^\dagger a}}{2}\mathcal{L}[c^\dagger a]$ [30] to model the incoherent exciton-cavity feeding. Figure 1a illustrates the energy-level diagram of the exciton and cavity system. The dissipator $\mathcal{L}[\xi] = \xi\rho\xi^\dagger - \frac{1}{2}\xi^\dagger\xi\rho - \frac{1}{2}\rho\xi^\dagger\xi$ with Lindblad operators ξ describes the cavity decay rate (κ), exciton decay rate (γ), and the incoherent phonon-mediated exciton-cavity scattering ($\Gamma_{ph}^{a^\dagger c}, \Gamma_{ph}^{c^\dagger a}$).

The phonon-mediated exciton-cavity scattering (Fig. 1b) with cavity-exciton detuning $\Delta_{CX} = \omega_C - \omega_X$ is given by

$$\Gamma_{ph}^{a^\dagger c/c^\dagger a} = 2\langle B \rangle^2 g^2 \text{Re} \left[\int_0^\infty d\tau e^{\pm\Delta_{CX}\tau} (e^{\phi(\tau)} - 1) \right] \quad (2)$$

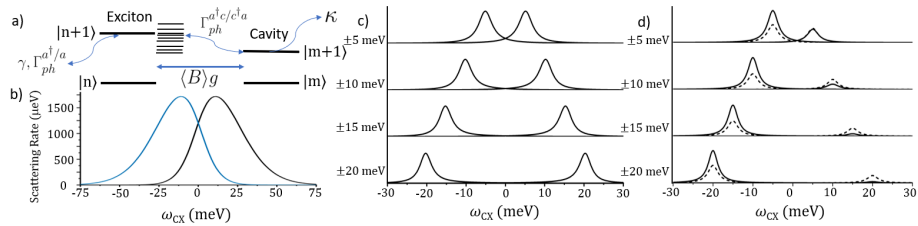


Figure 1: Theoretical modeling with the Hamiltonian described in the text ($T = 80$ K, $\gamma = 48.4$ meV, $\alpha_p = 0.018$ ps², $\omega_b = 6.7$ meV, $\kappa = 2.85$ meV, $g = 4$ meV) a) Level diagram with phonon-mediated scattering. b) Asymmetric phonon-mediated exciton-cavity coupling rates. The blue line gives the phonon-mediated incoherent emission into the cavity. Note that the peak is not centered at zero detuning. c) Detuning dependent ($\Delta_{CX} = \pm 5, \pm 10, \pm 15, \pm 20$ meV) cavity emission without phonons. d) Detuning dependent cavity emission with phonons at 80 K (solid line) and 320 K (dashed line). Note that for the $\Delta_{CX} = \pm 5$ meV the dashed and solid line are on top of each other for the blue detuned case.

with the phonon correlation function [31, 39]

$$\phi(\tau) = \int_0^\infty d\omega \frac{J(\omega)}{\omega^2} \left[\coth\left(\frac{\hbar\omega}{2k_B T}\right) \cos(\omega\tau) - i \sin(\omega\tau) \right]$$

We assume a Gaussian localization of the exciton confined to the monolayer TMDC due to substrate inhomogeneities for a qualitative super-ohmic spectral density $J(\omega) = \alpha_p \omega^3 \exp(-\omega^2/2\omega_b^2)$ [28, 31] with α_p and ω_b serving as the exciton-phonon coupling strength and cutoff frequency, respectively. This phonon spectral function is identical to that used in quantum dot studies of phonon interactions [36, 40, 41].

Without phonon-mediated scattering the peak cavity intensity occurs at zero detuning ($\omega_C = \omega_X$) and the cavity-coupled PL is symmetric with respect to the exciton PL emission peak (Fig. 1c). The additional scattering from phonon processes of the exciton into the cavity mode dominates when the cavity is red-detuned with respect to the exciton (Fig. 1d). Physically, we expect down-conversion of an exciton into a phonon and cavity photon as an example of a Stokes process. The opposite up-conversion amounts to optical refrigeration [42]. Including phonon-mediated scattering demonstrates the peak cavity intensity is red-detuned with respect to the exciton PL emission peak. Furthermore, our model predicts that at the same detuning, the relative intensity between the red-detuned and blue-detuned cavity-coupled photoluminescence decreases for increasing temperature (Fig. 1d, dashed line) [30].

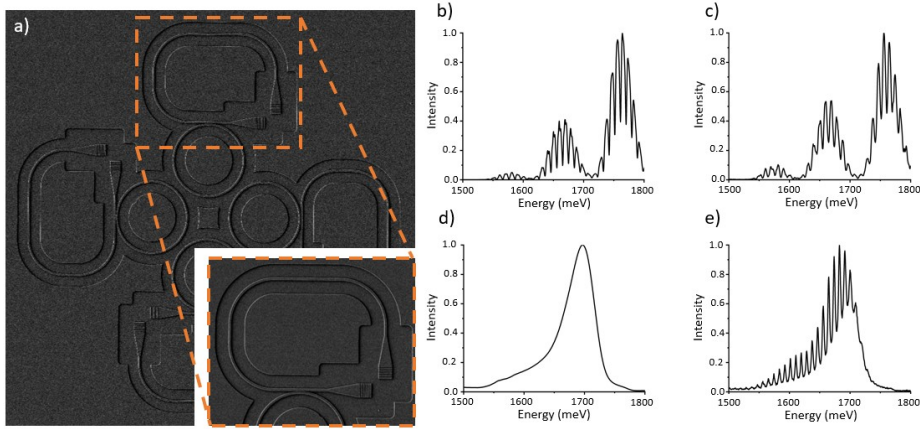


Figure 2: a) SEM of four 5 μm (radius) uncoupled SiN ring resonators. Inset: SEM of the coupled ring/waveguide and grating couplers. The grating couplers are used to input light and collect transmitted light. b) Transmission spectrum of the SiN ring resonator before integration of monolayer WSe₂. c) Transmission spectrum of the SiN ring resonator after integration of monolayer WSe₂. d) PL of monolayer WSe₂. e) Cavity-coupled PL of monolayer WSe₂.

3 Exciton-Cavity Photoluminescence Spectra

To validate our quantum optical model, we performed experiments with a ring resonator integrated with a monolayer of WSe₂. A ring resonator can support multiple cavity modes separated by the free spectral range, and thus provides an ideal platform for studying the coupling of the photoluminescence to cavity modes with different detunings from the exciton. The ring resonator is fabricated using a 220 nm thick silicon nitride (SiN) membrane grown via low pressure chemical vapor deposition (LPCVD) on 4 μm of thermal oxide on silicon. We spun roughly 400 nm of Zeon ZEP520A, which was coated with a thin layer of Pt/Au that served as a charging layer. The resist was patterned using a JEOL JBX6300FX electron-beam lithography system with an accelerating voltage of 100 kV. The pattern was transferred to the SiN using a reactive ion etch (RIE) in CHF₃/O₂ chemistry. The mechanically exfoliated WSe₂ was then transferred onto the SiN ring resonator (Fig. 2a) using a modified dry transfer method to eliminate bulk material contamination [26] which would otherwise quench the optical properties of the waveguide structures.

The transmission spectrum of the SiN ring resonator is measured by exciting a grating coupler with a supercontinuum laser (Fianium WhiteLase Micro) and collecting from the other grating coupler (Fig. 2a, inset). An initial transmission measurement of the ring resonator before monolayer TMDC transfer yields the bare cavity linewidth of $\kappa = 2.85$ meV (Fig. 2b). The dips in the transmission correspond to the resonance in the ring resonators. The separation between

the modes corresponds to the free spectral range ($\text{FSR} = \frac{c}{2\pi n_{\text{eff}} R} \approx 4.8 \text{ THz}$) of the ring resonator, which matches the FSR expected from the ring radius ($R = 5 \text{ }\mu\text{m}$) and effective index of refraction of the SiN waveguide ($n_{\text{eff}} \approx 2$). The envelope modulation of the spectrum is due to the frequency-dependent coupling efficiency of the grating couplers (Figs. 2b and 2c). The angular dependence of the grating coupler does not affect the cavity-coupled PL measurement due to the large numerical aperture of our objective lens. There exists a relative amplitude change between the envelope modulation function in the observed transmission spectrum due to the angular dependence of the grating couplers. As the measurement is done before and after the transfer, which requires removing the sample from the optical setup, the angular alignment of the confocal microscope objective to the grating coupler will be slightly different [43]. The transmission spectrum of the ring resonator after material transfer demonstrates the monolayer does not significantly affect the cavity modes (Fig. 2c). It is important to point out that with the exciton at approximately 1700 meV, the small linewidth increase seen in the transmission spectrum equally affects cavity modes both red and blue-detuned with respect to the exciton resonance.

Photoluminescence was first measured to confirm the existence of the monolayer after material transfer because 2D materials exhibit poor optical contrast on the SiN substrate (Fig. 2d). The strong excitonic peak of the WSe₂ monolayer integrated onto the SiN ring resonator establishes the presence of the vdW material on the waveguide [44]. The primary peak is attributed to neutral exciton emission. The secondary sidebands could be due to defects or trion emission [45, 46]. PL is measured by exciting the monolayer with a HeNe laser (40 μW at 633 nm). By fitting the measured PL at 80 K, the material dependent parameters for the phonon spectral function can be calculated, independent of the cavity coupling (Supplementary Materials). We found an exciton linewidth $\gamma = 48.4 \text{ meV}$, an exciton-phonon coupling $\alpha_p = 0.018 \text{ ps}^2$, and cutoff frequency $\omega_b = 6.7 \text{ meV}$. These extracted parameters are consistent with values estimated from bulk material measurements (Supplementary Materials). The polaron shift of the exciton energy is then calculated to be $\hbar\Delta_P = \hbar \int_0^\infty d\omega J(\omega)/\omega = \hbar \sqrt{\frac{\pi}{2}} \alpha_p \omega_b^3 = 24 \text{ meV}$, which we incorporate into the modified exciton resonance $\Delta'_{xL} = \Delta_{xL} - \Delta_P$.

Cavity-coupled PL is measured by directly exciting the monolayer WSe₂ from the top and collecting the resulting emission from a grating coupler using a pinhole in the image plane of a free-space confocal microscope. Cavity-coupled PL exhibits asymmetric emission into the cavity modes where there is greater intensity in the cavities red-detuned with respect to the exciton (Fig. 2e). The coherent exciton-cavity coupling $\hbar g$ can be extracted by considering the linear superposition of all cavity resonances for the ring resonator and including a contribution from background PL that is difficult to completely remove due to the proximity of the grating coupler and laser excitation of the monolayer WSe₂. The exciton-cavity coupling accounting for the average phonon displacement is found to be $\hbar g \approx 4 - 6 \text{ meV}$ (Fig. 3) by a brute force search minimizing the

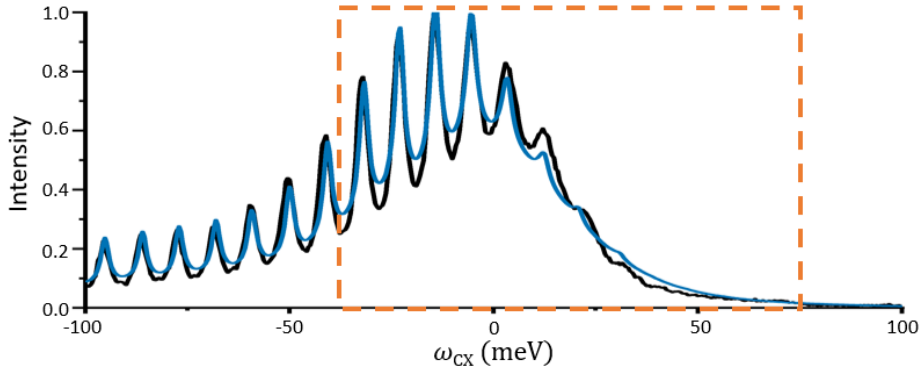


Figure 3: Measured cavity-coupled PL (black) and simulated cavity-coupled PL (blue) at 80 K. Theoretical model fit to the windowed region of data with the Hamiltonian described in the text ($T = 80$ K, $\gamma = 48.4$ meV, $\alpha_p = 0.018$ ps⁻², $\omega_b = 6.7$ meV, $\kappa = 2.85$ meV, $g = 4$ meV).

least squares error between the simulated and observed data over a windowed region of the cavity-coupled PL spectrum. The far red-detuned data attributed to defect and trion emission was accounted for by a convolution of the PL and Lorentzian cavity modes (Supplementary Materials). In this experiment only $\sim 1/4$ of the SiN ring resonator was covered with monolayer WSe₂. A full coverage of monolayer WSe₂ on the SiN ring resonator gives $\hbar g \approx 8 - 12$ meV as an estimated coherent interaction of the exciton and cavity mode due to the $g \propto \sqrt{N}$ scaling of the light-matter interaction in the collective excitation basis and assuming the number of available exciton states is proportional to the area of monolayer material on the cavity. Our extracted g value is consistent with the light-matter interaction $g \approx 10 - 14$ meV found in strong-coupling experiments with van der Waals materials integrated on photonic crystal cavities with comparable length of the cavity [12, 47, 48]. We note that for the ring resonator, the length of the cavity that goes into calculation of the g is the thickness of the slab (~ 220 nm).

To further confirm the theoretical model, we measure the temperature-dependent variation in the asymmetric coupling in the range 80 K - 320 K. Using liquid nitrogen in a continuous flow cryostat (Janis ST-500) we can tune the energy of the exciton in the monolayer WSe₂ from 1650 meV - 1700 meV with the consequent changes in linewidth. As the cryostat temperature is increased we see cavity-coupled PL extending to further blue-detuned cavities with respect to the exciton energy (Fig. 4a) where the spectra are shifted by the exciton center frequency. In particular, the maximum detuning with visible cavity modes increases with increasing temperature (Fig. 4b). We find the model Hamiltonian parameters extracted from the PL and cavity-coupled PL qualitatively reproduce the spectrum at elevated temperatures (Fig. 4c) where the only modified simulation parameter is the measured temperature of the

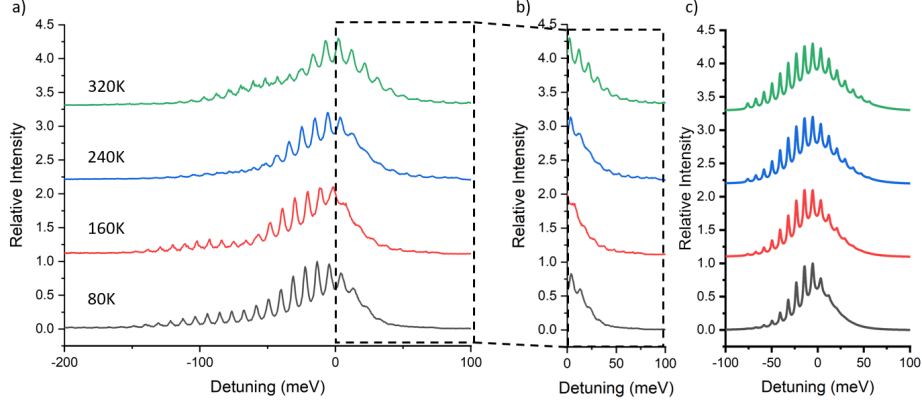


Figure 4: a) Temperature dependence (80 K to 320 K) of the asymmetric cavity-coupled PL. b) Zoomed-in to show the temperature dependence of the asymmetric cavity-coupled PL for cavities blue-detuned with respect to the exciton. c) Simulated temperature dependence of cavity-coupled PL without trion and defect emission. All free parameters are held fixed except the measured cryostat temperature ($T = 80$ K, 160 K, 240 K, 320 K, $\gamma = 48.4$ meV, $\alpha_p = 0.018$ ps², $\omega_b = 6.7$ meV, $\kappa = 2.85$ meV, $g = 4$ meV).

cryostat. Reduced asymmetry in cavity-coupled PL at elevated temperatures is due to the reduced asymmetry of the phonon-mediated exciton-cavity coupling rates with respect to the neutral exciton resonance.

4 Conclusion

We have explored exciton-phonon interactions in cavity-integrated TMDCs and demonstrated that a phenomenological deformation potential has significant value in explaining asymmetric cavity emission [6, 7, 25, 26]. Reflecting on the effective system Hamiltonian (Eq. 1), the polaron shift $\Delta_P = 24$ meV of the exciton energy is comparable to the $\Delta_P = 29$ meV found via the excitonic Bloch equations [19]. Temperature dependence of the exciton-cavity coupling has been previously observed in strong-coupling experiments with TMDC excitons [12, 48, 49], although a rigorous model explaining this behavior was not reported. We attribute this modification of the bare value to the average phonon displacement $g \rightarrow \langle B \rangle g$. A consequence of the exciton-cavity incoherent scattering (Eq. 2) is an efficient means for exciton population inversion which could potentially explain observations of lasing in cavity-integrated monolayer materials [5, 6, 7, 8, 30, 50]. In the interest of a low-power optical non-linearity, polaron-polaron scattering in the effective system Hamiltonian ($\Delta_P a^\dagger a^\dagger a a$) provides an interesting opportunity which could lead to non-classical light generation [33]. The calculated polaron shift is two orders of magnitude larger than expected for exciton-exciton scattering due to a lateral confining potential [14]. A full

understanding of the many-body interactions in nanocavity-integrated monolayer transition metal dichalcogenides is a necessary prerequisite to assessing the potential of this system for future classical and quantum technologies.

5 Acknowledgments

The research was supported by NSF-1845009, NSF-ECCS-1708579 and AFOSR grant FA9550-17-C-0017. Part of this work was conducted at the Washington Nanofabrication Facility / Molecular Analysis Facility, a National Nanotechnology Coordinated Infrastructure (NNCI) site at the University of Washington, which is supported in part by funds from the National Science Foundation (awards NNCI-1542101, 1337840 and 0335765), the National Institutes of Health, the Molecular Engineering & Sciences Institute, the Clean Energy Institute, the Washington Research Foundation, the M. J. Murdock Charitable Trust, Altatech, ClassOne Technology, GCE Market, Google and SPTS. A.R. acknowledges support from the IC Postdoctoral Research Fellowship.

Supplementary Materials: Exciton-phonon interactions in nanocavity-integrated monolayer transition metal dichalcogenides

1 Polaron Transformation

The microscopic Hamiltonian description of our system begins with a coupled oscillator model H_{XC} wherein the exciton $\Delta_{XL} = \omega_X - \omega_L$ and cavity $\Delta_{CL} = \omega_C - \omega_L$ resonances, measured with respect to the laser frequency ω_L , interact via an exciton-cavity coupling g [14, 27]. The deformation potential exciton-phonon interaction (H_{XP}) [28, 29] is a simplified model to account for effects of the solid state environment. Although we are interested in incoherent excitation for this experiment we will later argue for a coherent driving term for the exciton η_X in photoluminescence. The total Hamiltonian is $H = H_{XC} + H_D + H_{XP}$ with components

$$H_{XC} = \hbar\Delta_{XL}a^\dagger a + \hbar\Delta_{CL}c^\dagger c + \hbar g(a^\dagger c + c^\dagger a) \quad (S1)$$

$$H_D = \hbar\eta_X(a + a^\dagger) \quad (S2)$$

$$H_{XP} = \hbar a^\dagger a \sum_q \lambda_q (b_q + b_q^\dagger) + \sum_q \hbar\omega_q b_q^\dagger b_q \quad (S3)$$

The polaron transformation $P = a^\dagger a \sum_q \frac{\lambda_q}{\omega_q} (b_q^\dagger - b_q)$ with $H \rightarrow e^P H e^{-P}$ [32, 34] using the identity $e^X Y e^{-X} = Y + [X, Y] + \frac{1}{2!}[X, [X, Y]] + \frac{1}{3!}[X, [X, [X, Y]]] + \dots$ and $a, b,$ and c are all bosonic operators (e.g. $[a, a^\dagger] = 1$) leads to

$$\begin{aligned} \Delta_{XL}a^\dagger a &\rightarrow \Delta_{XL}a^\dagger a \\ \Delta_{CL}c^\dagger c &\rightarrow \Delta_{CL}c^\dagger c \\ a^\dagger a \sum_q \lambda_q (b_q + b_q^\dagger) &\rightarrow a^\dagger a \sum_q \lambda_q (b_q + b_q^\dagger) - 2(a^\dagger a)^2 \sum_q \frac{\lambda_q^2}{\omega_q} \\ &= a^\dagger a \sum_q \lambda_q (b_q + b_q^\dagger) - 2(a^\dagger a)^2 \Delta_P \\ \sum_q \omega_q b_q^\dagger b_q &\rightarrow \sum_q \omega_q b_q^\dagger b_q - a^\dagger a \sum_q \lambda_q (b_q + b_q^\dagger) + (a^\dagger a)^2 \sum_q \frac{\lambda_q^2}{\omega_q} \\ &= \sum_q \omega_q b_q^\dagger b_q - a^\dagger a \sum_q \lambda_q (b_q + b_q^\dagger) + (a^\dagger a)^2 \Delta_P \end{aligned}$$

$$\begin{aligned}
& g(a^\dagger c + c^\dagger a) + \eta_X(a + a^\dagger) \rightarrow g(a^\dagger c + c^\dagger a) + \eta_X(a + a^\dagger) \\
& + \left[\sum_q \frac{\lambda_q}{\omega_q} (b_q^\dagger - b_q) \right] [g(a^\dagger c - c^\dagger a) + \eta_X(a - a^\dagger)] \\
& + \left[\sum_q \frac{\lambda_q}{\omega_q} (b_q^\dagger - b_q) \right]^2 [g(a^\dagger c + c^\dagger a) + \eta_X(a + a^\dagger)] \\
& + \left[\sum_q \frac{\lambda_q}{\omega_q} (b_q^\dagger - b_q) \right]^3 [g(a^\dagger c - c^\dagger a) + \eta_X(a - a^\dagger)] + \dots \\
& = \exp \left[\sum_q \frac{\lambda_q}{\omega_q} (b_q^\dagger - b_q) \right] (g a^\dagger c + \eta_X a) + \exp \left[- \sum_q \frac{\lambda_q}{\omega_q} (b_q^\dagger - b_q) \right] (g c^\dagger a + \eta_X a^\dagger) \\
& = g \underbrace{(B_+ a^\dagger c)}_1 + \underbrace{(B_- c^\dagger a)}_2 + \eta_X \underbrace{(B_+ a^\dagger)}_3 + \underbrace{(B_- a)}_4 \\
& = \frac{1}{2} \left[\underbrace{g B_+ c^\dagger a}_I + \underbrace{g B_+ a^\dagger c}_I + \underbrace{\eta_X B_+ a}_{III} + \underbrace{\eta_X B_+ a^\dagger}_3 \right. \\
& + \underbrace{g B_- c^\dagger a}_2 + \underbrace{g B_- a^\dagger c}_{II} + \underbrace{\eta_X B_- a}_4 + \underbrace{\eta_X B_- a^\dagger}_{IV} \\
& + \underbrace{g B_+ a^\dagger c}_1 - \underbrace{g B_+ c^\dagger a}_I + \underbrace{\eta_X B_+ a^\dagger}_3 - \underbrace{\eta_X B_+ a}_{III} \\
& \left. - \underbrace{g B_- a^\dagger c}_{II} + \underbrace{g B_- c^\dagger a}_2 - \underbrace{\eta_X B_- a^\dagger}_{IV} + \underbrace{\eta_X B_- a}_4 \right] \\
& = \frac{1}{2} (B_+ + B_-) [g(c^\dagger a + a^\dagger c) + \eta_X(a + a^\dagger)] \\
& + \frac{1}{2} (B_+ - B_-) [g(a^\dagger c - c^\dagger a) + \eta_X(a^\dagger - a)] \\
& = \frac{1}{2} (B_+ + B_-) X_g + \frac{1}{2i} (B_+ - B_-) X_u \\
& = \frac{1}{2} (B_+ + B_- - 2\langle B \rangle) X_g + \langle B \rangle X_g + \frac{1}{2i} (B_+ - B_-) X_u \\
& = \zeta_g X_g + \zeta_u X_u + \langle B \rangle X_g
\end{aligned}$$

We define the polaron shift $\Delta_P = \sum_q \frac{\lambda_q^2}{\omega_q} = \int_0^\infty d\omega J(\omega)/\omega$ and the exciton-cavity coupling terms

$$\begin{aligned}
X_g &= \hbar g(c^\dagger a + a^\dagger c) + \hbar \eta_X(a + a^\dagger) \\
X_u &= i\hbar g(a^\dagger c - c^\dagger a) + i\hbar \eta_X(a^\dagger - a)
\end{aligned}$$

$J(\omega)$ is the phonon spectral function discussed in the main text. The bath displacement operators $B_\pm = \exp \left[\pm \sum_q \frac{\lambda_q}{\omega_q} (b_q - b_q^\dagger) \right]$ are included in the exciton-

cavity prefactors

$$\zeta_g = \frac{1}{2}(B_+ + B_- - 2\langle B \rangle)$$

$$\zeta_u = \frac{1}{2i}(B_+ - B_-)$$

where $\langle B \rangle = \langle B_+ \rangle = \langle B_- \rangle$. The resulting system, bath, and interaction Hamiltonian give

$$H'_S = \hbar\Delta_{XL}a^\dagger a - \hbar\Delta_P(a^\dagger a)^2 + \hbar\Delta_{CL}c^\dagger c + \langle B \rangle X_g \quad (\text{S4})$$

$$= \hbar(\Delta_{XL} - \Delta_P)a^\dagger a - \hbar\Delta_P a^\dagger a^\dagger a a + \hbar\Delta_{CL}c^\dagger c + \langle B \rangle X_g \quad (\text{S5})$$

$$H'_B = \sum_q \hbar\omega_q b_q^\dagger b_q \quad (\text{S6})$$

$$H'_I = X_g \zeta_g + X_u \zeta_u \quad (\text{S7})$$

2 Effective Phonon Master Equation

We use the Markovian time-convolutionless (TCL) master equation to approximate the temporal dynamics of our system [32, 36, 38, 39, 51, 52].

$$\frac{\partial \rho(t)}{\partial t} = \frac{1}{i\hbar} [H'_S, \rho(t)] + \mathcal{L}(\rho) - \frac{1}{\hbar^2} \int_0^\infty d\tau \sum_{m=g,u} \{G_m(\tau) [\hat{X}_m, e^{-iH'_S\tau/\hbar} \hat{X}_m e^{iH'_S\tau/\hbar} \rho(t)] + H.c.\} \quad (\text{S8})$$

$G_m(t)$ are the polaron Green functions ($m = g, u$)

$$G_g(t) = \langle B \rangle^2 \cosh[\phi(t)] - 1$$

$$G_u(t) = \langle B \rangle^2 \sinh[\phi(t)]$$

and $\phi(\tau) = \int_0^\infty d\omega \frac{J(\omega)}{\omega^2} \left[\coth\left(\frac{\hbar\omega}{2k_B T}\right) \cos(\omega\tau) - i \sin(\omega\tau) \right]$ is the phonon correlation function. The average phonon displacement can be calculated as $\langle B \rangle = \exp(-\phi(0)/2)$ [52].

To approximate the integral in the master equation we assume the cavity-exciton detuning (Δ_{CX}) is large compared to g and weak excitation such that $\langle a^\dagger a \rangle \ll 1$. We can then say

$$e^{-iH'_S\tau/\hbar} \hat{X}_m e^{iH'_S\tau/\hbar} \simeq e^{-iH'_0\tau/\hbar} \hat{X}_m e^{iH'_0\tau/\hbar} \quad (\text{S9})$$

with $H'_0 = \hbar(\Delta_{XL} - \Delta_P)a^\dagger a + \hbar\Delta_{CL}c^\dagger c$ where we renormalize $\Delta_{XL} - \Delta_P \rightarrow$

Δ_{XL} . The component transformations become

$$\begin{aligned}
e^{-iH'_0\tau/\hbar} a e^{iH'_0\tau/\hbar} &= a^\dagger e^{-i\Delta_{XL}\tau} \\
e^{-iH'_0\tau/\hbar} a^\dagger e^{iH'_0\tau/\hbar} &= a^\dagger e^{i\Delta_{XL}\tau} \\
e^{-iH'_0\tau/\hbar} c^\dagger a e^{iH'_0\tau/\hbar} &= c^\dagger e^{i\Delta_{CL}\tau} a e^{-i\Delta_{XL}\tau} \\
&= c^\dagger a e^{-i\Delta_{CX}\tau} \\
e^{-iH'_0\tau/\hbar} a^\dagger c e^{iH'_0\tau/\hbar} &= a^\dagger e^{i\Delta_{XL}\tau} c e^{-i\Delta_{CL}\tau} \\
&= a^\dagger c e^{i\Delta_{CX}\tau}
\end{aligned}$$

Without the coherent driving term, substitution gives

$$\begin{aligned}
& G_g(\tau)[\hat{X}_g, e^{-iH'_S\tau/\hbar}\hat{X}_g e^{iH'_S\tau/\hbar}\rho(t)] + H.c. \\
& \simeq \hbar^2 g^2 G_g(\tau)(c^\dagger a + a^\dagger c)(c^\dagger a e^{i\Delta_{CX}\tau} + a^\dagger c e^{-i\Delta_{CX}\tau})\rho(t) \\
& - \hbar^2 g^2 G_g(\tau)(c^\dagger a e^{i\Delta_{CX}\tau} + a^\dagger c e^{-i\Delta_{CX}\tau})\rho(t)(c^\dagger a + a^\dagger c) \\
& + \hbar^2 g^2 G_g^*(\tau)\rho(t)(c^\dagger a e^{-i\Delta_{CX}\tau} + a^\dagger c e^{i\Delta_{CX}\tau})(c^\dagger a + a^\dagger c) \\
& - \hbar^2 g^2 G_g^*(c^\dagger a + a^\dagger c)\rho(t)(c^\dagger a e^{-i\Delta_{CX}\tau} + a^\dagger c e^{i\Delta_{CX}\tau}) \\
& = \hbar^2 g^2 \{ \underbrace{G_g(\tau) e^{-i\Delta_{CX}\tau} a^\dagger c c^\dagger a \rho(t)}_1 + \underbrace{G_g(\tau) e^{i\Delta_{CX}\tau} c^\dagger a a^\dagger c \rho(t)}_5 \\
& - \hbar^2 g^2 [\underbrace{G_g(\tau) e^{-i\Delta_{CX}\tau} c^\dagger a \rho(t) a^\dagger c}_3 + \underbrace{G_g(\tau) e^{i\Delta_{CX}\tau} a^\dagger c \rho(t) c^\dagger a}_7] \\
& + \hbar^2 g^2 [\underbrace{G_g^*(\tau) e^{-i\Delta_{CX}\tau} \rho(t) c^\dagger a a^\dagger c}_6 + \underbrace{G_g^*(\tau) e^{i\Delta_{CX}\tau} \rho(t) a^\dagger c c^\dagger a}_2] \\
& - \hbar^2 g^2 [\underbrace{G_g^*(\tau) e^{-i\Delta_{CX}\tau} a^\dagger c \rho(t) c^\dagger a}_8 + \underbrace{G_g^*(\tau) e^{i\Delta_{CX}\tau} c^\dagger a \rho(t) a^\dagger c}_4] \\
& = \hbar^2 g^2 \{ \underbrace{\Re[G_g(\tau) e^{-i\Delta_{CX}\tau}] a^\dagger c c^\dagger a \rho(t) + i \Im[G_g(\tau) e^{-i\Delta_{CX}\tau}] a^\dagger c c^\dagger a \rho(t)}_1 \\
& + \hbar^2 g^2 \{ \underbrace{\Re[G_g(\tau) e^{-i\Delta_{CX}\tau}] \rho(t) a^\dagger c c^\dagger a - i \Im[G_g(\tau) e^{-i\Delta_{CX}\tau}] \rho(t) a^\dagger c c^\dagger a}_2 \\
& - \hbar^2 g^2 \{ \underbrace{G_g(\tau) e^{-i\Delta_{CX}\tau} c^\dagger a \rho(t) a^\dagger c}_3 + \underbrace{G_g^*(\tau) e^{i\Delta_{CX}\tau} c^\dagger a \rho(t) a^\dagger c}_4 \} \\
& + \hbar^2 g^2 \{ \underbrace{\Re[G_g(\tau) e^{i\Delta_{CX}\tau}] c^\dagger a a^\dagger c \rho(t) + i \Im[G_g(\tau) e^{i\Delta_{CX}\tau}] c^\dagger a a^\dagger c \rho(t)}_5 \\
& + \hbar^2 g^2 \{ \underbrace{\Re[G_g(\tau) e^{i\Delta_{CX}\tau}] \rho(t) c^\dagger a a^\dagger c - i \Im[G_g(\tau) e^{i\Delta_{CX}\tau}] \rho(t) c^\dagger a a^\dagger c}_6 \\
& - \hbar^2 g^2 \{ \underbrace{G_g(\tau) e^{i\Delta_{CX}\tau} a^\dagger c \rho(t) c^\dagger a}_7 + \underbrace{G_g^*(\tau) e^{-i\Delta_{CX}\tau} a^\dagger c \rho(t) c^\dagger a}_8 \}
\end{aligned}$$

$$\begin{aligned}
& G_g(\tau)[\hat{X}_g, e^{-iH'_s\tau/\hbar}\hat{X}_g e^{iH'_s\tau/\hbar}\rho(t)] + H.c. \\
& \simeq \hbar^2 g^2 \Re[G_g(\tau)e^{-i\Delta_{CX}\tau}](\underbrace{a^\dagger c c^\dagger a \rho(t)}_{\Re[1]} + \underbrace{\rho(t) a^\dagger c c^\dagger a}_{\Re[2]} - \underbrace{2c^\dagger a \rho(t) a^\dagger c}_{3+4}) \\
& + \hbar^2 g^2 \Re[G_g(\tau)e^{i\Delta_{CX}\tau}](\underbrace{c^\dagger a a^\dagger c \rho(t)}_{\Re[5]} + \underbrace{\rho(t) c^\dagger a a^\dagger c}_{\Re[6]} - \underbrace{2a^\dagger c \rho(t) c^\dagger a}_{7+8}) \\
& + i\hbar^2 g^2 \Im[G_g(\tau)e^{-i\Delta_{CX}\tau}](\underbrace{a^\dagger c c^\dagger a \rho(t)}_{\Im[1]} - \underbrace{\rho(t) a^\dagger c c^\dagger a}_{\Im[2]}) \\
& + i\hbar^2 g^2 \Im[G_g(\tau)e^{i\Delta_{CX}\tau}](\underbrace{c^\dagger a a^\dagger c \rho(t)}_{\Im[5]} - \underbrace{\rho(t) c^\dagger a a^\dagger c}_{\Im[6]})
\end{aligned}$$

We lose eight terms in the first equality by cancellation with terms from the integrand containing X_u due to the imaginary i giving an overall minus sign to the manipulations. By inspection of the last equality all c^\dagger are replaced by $-c^\dagger$ for the integrand with $X_u(\tau)$ but the overall minus sign negates this. We can then sum over $m = g, u$.

$$\begin{aligned}
& g^2 \int_0^\infty d\tau \sum_{m=g,u} \{ \Re[G_m(\tau)e^{-i\Delta_{CX}\tau}](a^\dagger c c^\dagger a \rho(t) + \rho(t) a^\dagger c c^\dagger a - 2c^\dagger a \rho(t) a^\dagger c) \\
& \quad + \Re[G_m(\tau)e^{i\Delta_{CX}\tau}](c^\dagger a a^\dagger c \rho(t) + \rho(t) c^\dagger a a^\dagger c - 2a^\dagger c \rho(t) c^\dagger a) \\
& \quad + i\Im[G_m(\tau)e^{-i\Delta_{CX}\tau}](a^\dagger c c^\dagger a \rho(t) - \rho(t) a^\dagger c c^\dagger a) \\
& \quad + i\Im[G_m(\tau)e^{i\Delta_{CX}\tau}](c^\dagger a a^\dagger c \rho(t) - \rho(t) c^\dagger a a^\dagger c) \}
\end{aligned}$$

Recall $\sum_{m=g,u} G_m(\tau) = \langle B \rangle^2 (e^{\phi(\tau)} - 1)$ and the dissipator is defined $\mathcal{L}(\xi) = \xi \rho \xi^\dagger - \frac{1}{2} \xi^\dagger \xi \rho - \frac{1}{2} \rho \xi^\dagger \xi$ with Lindbladian operators ξ . The resulting term becomes

$$i[\Delta_{ph}^{a^\dagger c} a^\dagger c c^\dagger a + \Delta_{ph}^{c^\dagger a} c^\dagger a a^\dagger c, \rho(t)] + \frac{\Gamma_{ph}^{a^\dagger c}}{2} \mathcal{L}(a^\dagger c) + \frac{\Gamma_{ph}^{c^\dagger a}}{2} \mathcal{L}(c^\dagger a) \quad (\text{S10})$$

The frequency shifts are given

$$\Delta_{ph}^{a^\dagger c/c^\dagger a} = \langle B \rangle^2 g^2 \text{Im} \left[\int_0^\infty d\tau e^{\pm i\Delta_{CX}\tau} (e^{\phi(\tau)} - 1) \right] \quad (\text{S11})$$

The scattering rates are given

$$\Gamma_{ph}^{a^\dagger c/c^\dagger a} = 2\langle B \rangle^2 g^2 \text{Re} \left[\int_0^\infty d\tau e^{\pm i\Delta_{CX}\tau} (e^{\phi(\tau)} - 1) \right] \quad (\text{S12})$$

If we ignore cross-terms in the integrand commutator between the coherent exciton-cavity interaction g and coherent exciton drive η_X we can avoid a re-derivation by observing we can remove all c and c^\dagger , replacing $g \rightarrow \eta_X$, and replacing $\Delta_{CX} \rightarrow \Delta_{XL}$. The resulting term becomes

$$i[\Delta_{ph}^{a^\dagger} a^\dagger a + \Delta_{ph}^a a a^\dagger, \rho(t)] + \frac{\Gamma_{ph}^{a^\dagger}}{2} \mathcal{L}(a^\dagger) + \frac{\Gamma_{ph}^a}{2} \mathcal{L}(a) \quad (\text{S13})$$

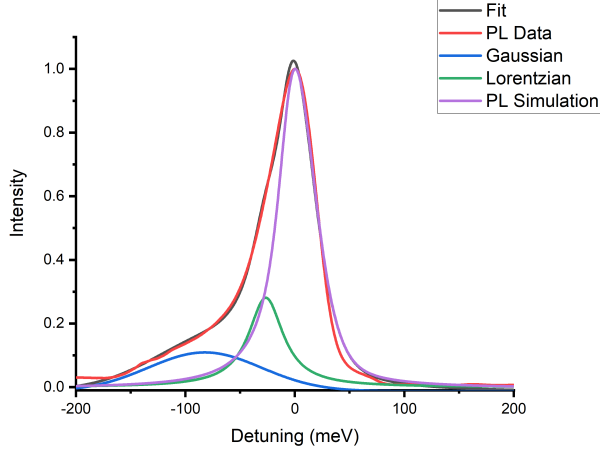


Figure S1: The extracted fit parameters for equation S17 are: $y_0 = -0.01262$, $A_D = 15.82$, $\Gamma_D = 122.0$ meV, $\Delta_D = -82.31$ meV, $A_T = 17.02$, $\Gamma_T = 38.56$ meV, $\Delta_T = -26.55$ meV, $f = 0.9038$, $\alpha_p = 0.018$ ps², and $\omega_b = 6.7$ meV.

The frequency shifts are given

$$\Delta_{ph}^{a^\dagger/a} = \langle B \rangle^2 \eta_X^2 \text{Im} \left[\int_0^\infty d\tau e^{\pm i \Delta_{XL} \tau} (e^{\phi(\tau)} - 1) \right] \quad (\text{S14})$$

The scattering rates are given

$$\Gamma_{ph}^{a^\dagger/a} = 2 \langle B \rangle^2 \eta_X^2 \text{Re} \left[\int_0^\infty d\tau e^{\pm i \Delta_{XL} \tau} (e^{\phi(\tau)} - 1) \right] \quad (\text{S15})$$

For the purposes of simulation and fitting to the data we choose to ignore the Stark shifts $\Delta_{ph}^{a^\dagger c/c^\dagger a}$ and $\Delta_{ph}^{a^\dagger/a}$.

3 Photoluminescence

Our experiments involve above-band excitation which phenomenologically amounts to an incoherent drive of the neutral exciton. Our presented simplified model requires a coherent drive for phonon-mediated processes as seen by the η_X in the $\Gamma_{ph}^{a^\dagger/a}$ scattering rates. If we represent the incoherent excitation as a coherent field with a random phase [53, 54, 55] the Markovian approximation made for the TCL master equation allows us to consider a steady state population of neutral excitons by effectively integrating out the transient dynamics.

The steady-state exciton population [56] without cavity-coupling can be

found for comparison to photoluminescent (PL) measurements

$$\bar{N}_X = \frac{1}{2} \left[1 + \frac{\Gamma_{ph}^{\sigma^+} - \Gamma_{ph}^{\sigma^-} - \gamma}{\Gamma_{ph}^{\sigma^+} + \Gamma_{ph}^{\sigma^-} + \gamma + \frac{4\eta_x^2 \langle B \rangle^2 \Gamma_{pol}}{\Gamma_{pol}^2 + \Delta_{XL}^2}} \right] \quad (\text{S16})$$

with $\Gamma_{pol} = \frac{1}{2}(\Gamma_{ph}^{\sigma^+} + \Gamma_{ph}^{\sigma^-} + \gamma)$. For numerical fitting of the data to this model we use $\eta_X = 0.01\gamma$. The coefficient choice does not significantly affect the lineshape of \bar{N}_x . Fixed parameters in this model are temperature (T) and the exciton decay rate (γ) extracted from the linewidth of the exciton resonance. \bar{N}_X reduces to a Lorentzian with full width at half maximum (FWHM) equal to γ . Free parameters of the model are the exciton-phonon coupling strength (α_p) and cutoff frequency (ω_b).

The secondary sidebands assumed to be defects or trions [45, 46] are fit using a Gaussian and Lorentzian function, respectively. The defect Gaussian function incorporates an inhomogenous broadening mechanism due to local perturbations. The trion Lorentzian function assumes only homogeneous broadening [18]. The total PL spectrum is fit using SciPy's *curve_fit* function for the Gaussian and Lorentzian terms, and a brute force grid search for α_p and ω_b .

$$S_{PL}(\Delta_{XL}) = y_0 + \frac{A_D e^{-\frac{4 \ln 2 (\Delta_{XL} - \Delta_D)^2}{\Gamma_D^2}}}{\Gamma_D \sqrt{\frac{\pi}{4 \ln 2}}} + \frac{2A_T}{\pi} \frac{\Gamma_T}{4(\Delta_{XL} - \Delta_T)^2 + \Gamma_T^2} + f\bar{N}_X(\Delta_{XL}) \quad (\text{S17})$$

The defect ($\Delta_D = -82.31$ meV) and trion ($\Delta_T = -26.55$ meV) peak detunings with respect to the neutral exciton are consistent with previous results in the literature ($\Delta_D \approx -101$ meV, $\Delta_T \approx -28$ meV) [45, 57].

Although there are excellent papers on the subject of phonon-mediated interactions in monolayer materials [15, 19, 20, 58], there is no clear comparison for α_p and ω_b . As a sanity check, α_p for a spherically confining potential is known to be $\frac{(D_c - D_v)^2}{4\pi^2 \rho s^5}$ [40, 41, 59]. D_c (D_v) are the deformation potential constants for the conduction (valence) band, ρ is the bulk material density, and s is the sound velocity. Using the bulk material parameters for WSe₂ with $|D_c - D_v| = 5.4$ eV [60], $\rho = 9.32$ g cm⁻³ [61], and $s = 4000$ m s⁻¹ [62] we find $\alpha_p = 0.019$ meV, which is similar to our extracted result of $\alpha_p = 0.018$ meV. The phonon cutoff energy $\omega_b = \frac{s}{d} = 6.7$ meV corresponds to a $d = 3$ nm in-plane localization. This length scale is not unreasonable for an estimate of the silicon nitride surface roughness. There may also be some correlation between the localization and defect emission.

4 Total Spectrum

The cavity-coupled PL spectrum is found from the Fourier transform of the correlation function

$$S(\omega) = \int_{-\infty}^{\infty} \lim_{t \rightarrow \infty} \langle c^\dagger(t + \tau)c(t) \rangle d\tau$$

which is provided as a function in the QuTiP Python library [63, 64]. Although it is tempting to simultaneously include all cavity resonances in the system Hamiltonian, with the cavity bosonic operator truncated at $N = 10$ to ensure convergence we quickly approach a Hilbert space dimension that is classically intractable to simulate. Instead, we recognize each cavity mode of the ring resonator can be treated independently because the spatial overlap of different modes is approximately equal to zero. Similarly, we only consider cavity modes which have the same spatial wavefunction as the collective excitation of the excitonic resonance [65, 66]. The total spectrum S_{Total} is then a linear superposition of all cavity resonances with different detuning Δ_{CX} coupled to the monolayer PL and background PL

$$\begin{aligned}
S_{Total}(\omega) &= f_1 S_{PL}(\omega) + f_2 \sum_{\Delta_{CX}} S_{\Delta_{CX}}(\omega) \\
&+ f_3 \frac{A_{De} \frac{-4 \ln 2 (\omega - \Delta_D)^2}{\Gamma_D^2}}{\Gamma_D \sqrt{\frac{\pi}{4 \ln 2}}} \sum_{\Delta_{CX}} \frac{2A_{DC}}{\pi} \frac{\Gamma_{DC}}{4(\omega - \Delta_{CX})^2 + \Gamma_{DC}^2} \\
&+ f_4 \frac{2A_T}{\pi} \frac{\Gamma_T}{4(\omega - \Delta_T)^2 + \Gamma_T^2} \sum_{\Delta_{CX}} \frac{2A_{TC}}{\pi} \frac{\Gamma_{TC}}{4(\omega - \Delta_{CX})^2 + \Gamma_{TC}^2}
\end{aligned}$$

The free parameters for fitting the model to the cavity-coupled PL data are f_{1-4} as the relative intensity of the background PL, cavity-coupled neutral exciton PL, cavity-coupled defect PL and cavity-coupled trion PL and the exciton-cavity coupling g . The relative intensity in our experiments is found to be $f_1 = 0.53$, $f_2 = 0.44$, $f_3 = 2.18$, and $f_4 = 1.49$. We chose a single cavity parameter for defect and trion emission to reduce overfitting. For the cavity-coupled defect PL $A_{DC} = 2.24$ and $\Gamma_{DC} = 2.33$ meV. For the cavity-coupled trion PL $A_{TC} = 1.42$ and $\Gamma_{TC} = 2.29$ meV.

References

- [1] Fengnian Xia, Han Wang, Di Xiao, Madan Dubey, and Ashwin Ramasubramanian. Two-dimensional material nanophotonics. *Nature Photonics*, 8(12):899–907, December 2014. ISSN 1749-4893. doi: 10.1038/nphoton.2014.271. URL <https://www.nature.com/articles/nphoton.2014.271>.
- [2] Yuan Liu, Nathan O. Weiss, Xidong Duan, Hung-Chieh Cheng, Yu Huang, and Xiangfeng Duan. Van der Waals heterostructures and devices. *Nature Reviews Materials*, 1(9):16042, September 2016. ISSN 2058-8437. doi: 10.1038/natrevmats.2016.42. URL <https://www.nature.com/articles/natrevmats201642>.
- [3] Chang-hua Liu, Jiajiu Zheng, Yueyang Chen, Taylor Fryett, and Arka Majumdar. Van der Waals materials integrated nanophotonic devices [Invited]. *Optical Materials Express*, 9(2):384–399, February 2019. ISSN 2159-

3930. doi: 10.1364/OME.9.000384. URL <https://www.osapublishing.org/ome/abstract.cfm?uri=ome-9-2-384>.
- [4] Taylor Fryett, Alan Zhan, and Arka Majumdar. Cavity nonlinear optics with layered materials. *Nanophotonics*, 7(2):355–370, 2018. doi: 10.1515/nanoph-2017-0069. URL <https://www.degruyter.com/view/j/nanoph.2018.7.issue-2/nanoph-2017-0069/nanoph-2017-0069.xml?lang=en>.
- [5] Sanfeng Wu, Sonia Buckley, John R. Schaibley, Liefeng Feng, Jiaqiang Yan, David G. Mandrus, Fariba Hatami, Wang Yao, Jelena Vučković, Arka Majumdar, and Xiaodong Xu. Monolayer semiconductor nanocavity lasers with ultralow thresholds. *Nature*, 520(7545):69–72, April 2015. ISSN 1476-4687. doi: 10.1038/nature14290. URL <https://www.nature.com/articles/nature14290>.
- [6] Yu Ye, Zi Jing Wong, Xiufang Lu, Xingjie Ni, Hanyu Zhu, Xianhui Chen, Yuan Wang, and Xiang Zhang. Monolayer excitonic laser. *Nature Photonics*, 9(11):733–737, November 2015. ISSN 1749-4893. doi: 10.1038/nphoton.2015.197. URL <https://www.nature.com/articles/nphoton.2015.197>.
- [7] Omid Salehzadeh, Mehrdad Djavid, Nhung Hong Tran, Ishiang Shih, and Zetian Mi. Optically Pumped Two-Dimensional MoS₂ Lasers Operating at Room-Temperature. *Nano Letters*, 15(8):5302–5306, August 2015. ISSN 1530-6984. doi: 10.1021/acs.nanolett.5b01665. URL <https://doi.org/10.1021/acs.nanolett.5b01665>.
- [8] Yongzhuo Li, Jianxing Zhang, Dandan Huang, Hao Sun, Fan Fan, Jibin Feng, Zhen Wang, and C. Z. Ning. Room-temperature continuous-wave lasing from monolayer molybdenum ditelluride integrated with a silicon nanobeam cavity. *Nature Nanotechnology*, 12(10):987–992, October 2017. ISSN 1748-3395. doi: 10.1038/nnano.2017.128. URL <https://www.nature.com/articles/nnano.2017.128>.
- [9] Taylor K. Fryett, Kyle L. Seyler, Jiajiu Zheng, Chang-Hua Liu, Xiaodong Xu, and Arka Majumdar. Silicon photonic crystal cavity enhanced second-harmonic generation from monolayer WSe₂. *2D Materials*, 4(1):015031, December 2016. ISSN 2053-1583. doi: 10.1088/2053-1583/4/1/015031. URL <https://doi.org/10.1088/2053-1583/4/1/015031>.
- [10] Xue-Tao Gan, Chen-Yang Zhao, Si-Qi Hu, Tao Wang, Yu Song, Jie Li, Qing-Hua Zhao, Wan-Qi Jie, and Jian-Lin Zhao. Microwatts continuous-wave pumped second harmonic generation in few- and mono-layer GaSe. *Light: Science & Applications*, 7(1):17126–17126, January 2018. ISSN 2047-7538. doi: 10.1038/lsa.2017.126. URL <https://www.nature.com/articles/lsa2017126>.
- [11] Chang-Hua Liu, Genevieve Clark, Taylor Fryett, Sanfeng Wu, Jiajiu Zheng, Fariba Hatami, Xiaodong Xu, and Arka Majumdar. Nanocavity Integrated van der Waals Heterostructure Light-Emitting Tunneling

- Diode. *Nano Letters*, 17(1):200–205, January 2017. ISSN 1530-6984. doi: 10.1021/acs.nanolett.6b03801. URL <https://doi.org/10.1021/acs.nanolett.6b03801>.
- [12] Long Zhang, Rahul Gogna, Will Burg, Emanuel Tutuc, and Hui Deng. Photonic-crystal exciton-polaritons in monolayer semiconductors. *Nature Communications*, 9(1):1–8, February 2018. ISSN 2041-1723. doi: 10.1038/s41467-018-03188-x. URL <https://www.nature.com/articles/s41467-018-03188-x>.
- [13] Valentin Walther, Robert Johne, and Thomas Pohl. Giant optical nonlinearities from Rydberg excitons in semiconductor microcavities. *Nature Communications*, 9(1):1–6, April 2018. ISSN 2041-1723. doi: 10.1038/s41467-018-03742-7. URL <https://www.nature.com/articles/s41467-018-03742-7>.
- [14] Albert Ryou, David Rosser, Abhi Saxena, Taylor Fryett, and Arka Majumdar. Strong photon antibunching in weakly nonlinear two-dimensional exciton-polaritons. *Physical Review B*, 97(23):235307, June 2018. doi: 10.1103/PhysRevB.97.235307. URL <https://link.aps.org/doi/10.1103/PhysRevB.97.235307>.
- [15] Galan Moody, Chandriker Kavir Dass, Kai Hao, Chang-Hsiao Chen, Lain-Jong Li, Akshay Singh, Kha Tran, Genevieve Clark, Xiaodong Xu, Gunnar Berghäuser, Ermin Malic, Andreas Knorr, and Xiaoqin Li. Intrinsic homogeneous linewidth and broadening mechanisms of excitons in monolayer transition metal dichalcogenides. *Nature Communications*, 6(1):1–6, September 2015. ISSN 2041-1723. doi: 10.1038/ncomms9315. URL <https://www.nature.com/articles/ncomms9315>.
- [16] C. Robert, D. Lagarde, F. Cadiz, G. Wang, B. Lassagne, T. Amand, A. Balocchi, P. Renucci, S. Tongay, B. Urbaszek, and X. Marie. Exciton radiative lifetime in transition metal dichalcogenide monolayers. *Physical Review B*, 93(20):205423, May 2016. doi: 10.1103/PhysRevB.93.205423. URL <https://link.aps.org/doi/10.1103/PhysRevB.93.205423>.
- [17] F. Cadiz, E. Courtade, C. Robert, G. Wang, Y. Shen, H. Cai, T. Taniguchi, K. Watanabe, H. Carrere, D. Lagarde, M. Manca, T. Amand, P. Renucci, S. Tongay, X. Marie, and B. Urbaszek. Excitonic Linewidth Approaching the Homogeneous Limit in MoS_2 -Based van der Waals Heterostructures. *Physical Review X*, 7(2):021026, May 2017. doi: 10.1103/PhysRevX.7.021026. URL <https://link.aps.org/doi/10.1103/PhysRevX.7.021026>.
- [18] Obafunso A. Ajayi, Jenny V. Ardelean, Gabriella D. Shepard, Jue Wang, Abhinandan Antony, Takeshi Taniguchi, Kenji Watanabe, Tony F. Heinz, Stefan Strauf, X.-Y. Zhu, and James C. Hone. Approaching the intrinsic photoluminescence linewidth in transition metal dichalcogenide monolayers. *2D Materials*, 4(3):031011, July 2017. ISSN 2053-1583. doi: 10.

1088/2053-1583/aa6aa1. URL <https://doi.org/10.1088%2F2053-1583%2Faa6aa1>.

- [19] Dominik Christiansen, Malte Selig, Gunnar Berghäuser, Robert Schmidt, Iris Niehues, Robert Schneider, Ashish Arora, Steffen Michaelis de Vasconcellos, Rudolf Bratschitsch, Ermin Malic, and Andreas Knorr. Phonon Sidebands in Monolayer Transition Metal Dichalcogenides. *Physical Review Letters*, 119(18):187402, November 2017. doi: 10.1103/PhysRevLett.119.187402. URL <https://link.aps.org/doi/10.1103/PhysRevLett.119.187402>.
- [20] S. Shree, M. Semina, C. Robert, B. Han, T. Amand, A. Balocchi, M. Manca, E. Courtade, X. Marie, T. Taniguchi, K. Watanabe, M. M. Glazov, and B. Urbaszek. Observation of exciton-phonon coupling in $\{\mathrm{MoSe}\}_2$ monolayers. *Physical Review B*, 98(3):035302, July 2018. doi: 10.1103/PhysRevB.98.035302. URL <https://link.aps.org/doi/10.1103/PhysRevB.98.035302>.
- [21] M. M. Glazov. Phonon wind and drag of excitons in monolayer semiconductors. *Physical Review B*, 100(4):045426, July 2019. doi: 10.1103/PhysRevB.100.045426. URL <https://link.aps.org/doi/10.1103/PhysRevB.100.045426>.
- [22] Arka Majumdar, Erik D. Kim, Yiyang Gong, Michal Bajcsy, and Jelena Vučković. Phonon mediated off-resonant quantum dot–cavity coupling under resonant excitation of the quantum dot. *Physical Review B*, 84(8):085309, August 2011. doi: 10.1103/PhysRevB.84.085309. URL <https://link.aps.org/doi/10.1103/PhysRevB.84.085309>.
- [23] Dirk Englund, Arka Majumdar, Andrei Faraon, Mitsuru Toishi, Nick Stoltz, Pierre Petroff, and Jelena Vučković. Resonant Excitation of a Quantum Dot Strongly Coupled to a Photonic Crystal Nanocavity. *Physical Review Letters*, 104(7):073904, February 2010. doi: 10.1103/PhysRevLett.104.073904. URL <https://link.aps.org/doi/10.1103/PhysRevLett.104.073904>.
- [24] S. Ates, S. M. Ulrich, A. Ulhaq, S. Reitzenstein, A. Löffler, S. Höfling, A. Forchel, and P. Michler. Non-resonant dot–cavity coupling and its potential for resonant single-quantum-dot spectroscopy. *Nature Photonics*, 3(12):724–728, December 2009. ISSN 1749-4893. doi: 10.1038/nphoton.2009.215. URL <https://www.nature.com/articles/nphoton.2009.215>.
- [25] Clément Javerzac-Galy, Anshuman Kumar, Ryan D. Schilling, Nicolas Piro, Sina Khorasani, Matteo Barbone, Ilya Goykhman, Jacob B. Khurgin, Andrea C. Ferrari, and Tobias J. Kippenberg. Excitonic Emission of Monolayer Semiconductors Near-Field Coupled to High-Q Microresonators. *Nano Letters*, 18(5):3138–3146, May 2018. ISSN 1530-6984. doi: 10.1021/acs.nanolett.8b00749. URL <https://doi.org/10.1021/acs.nanolett.8b00749>.

- [26] David Rosser, Taylor Fryett, Abhi Saxena, Albert Ryou, and Arka Majumdar. High-precision local transfer of van der Waals materials on nanophotonic structures. *arXiv:1908.01857 [cond-mat, physics:physics]*, July 2019. URL <http://arxiv.org/abs/1908.01857>. arXiv: 1908.01857.
- [27] J. C. López Carreño and F. P. Laussy. Excitation with quantum light. I. Exciting a harmonic oscillator. *Physical Review A*, 94(6):063825, December 2016. doi: 10.1103/PhysRevA.94.063825. URL <https://link.aps.org/doi/10.1103/PhysRevA.94.063825>.
- [28] T. Takagahara. Localization and energy transfer of quasi-two-dimensional excitons in GaAs-AlAs quantum-well heterostructures. *Physical Review B*, 31(10):6552–6573, May 1985. doi: 10.1103/PhysRevB.31.6552. URL <https://link.aps.org/doi/10.1103/PhysRevB.31.6552>.
- [29] Jai Singh. *Excitation Energy Transfer Processes in Condensed Matter: Theory and Applications*. Physics of Solids and Liquids. Springer US, 1994. ISBN 978-0-306-44780-8. doi: 10.1007/978-1-4899-0996-1. URL <https://www.springer.com/gp/book/9780306447808>.
- [30] S. Hughes and H. J. Carmichael. Phonon-mediated population inversion in a semiconductor quantum-dot cavity system. *New Journal of Physics*, 15(5):053039, May 2013. ISSN 1367-2630. doi: 10.1088/1367-2630/15/5/053039. URL <https://doi.org/10.1088/1367-2630/15/5/053039>.
- [31] A. J. Leggett, S. Chakravarty, A. T. Dorsey, Matthew P. A. Fisher, Anupam Garg, and W. Zwerger. Dynamics of the dissipative two-state system. *Reviews of Modern Physics*, 59(1):1–85, January 1987. doi: 10.1103/RevModPhys.59.1. URL <https://link.aps.org/doi/10.1103/RevModPhys.59.1>.
- [32] I. Wilson-Rae and A. Imamoglu. Quantum dot cavity-QED in the presence of strong electron-phonon interactions. *Physical Review B*, 65(23):235311, May 2002. doi: 10.1103/PhysRevB.65.235311. URL <https://link.aps.org/doi/10.1103/PhysRevB.65.235311>.
- [33] P. Rabl. Photon Blockade Effect in Optomechanical Systems. *Physical Review Letters*, 107(6):063601, August 2011. doi: 10.1103/PhysRevLett.107.063601. URL <https://link.aps.org/doi/10.1103/PhysRevLett.107.063601>.
- [34] R. E. Merrifield. Theory of the Vibrational Structure of Molecular Exciton States. *The Journal of Chemical Physics*, 40(2):445–450, January 1964. ISSN 0021-9606. doi: 10.1063/1.1725135. URL <https://aip.scitation.org/doi/10.1063/1.1725135>.
- [35] Gerald D. Mahan. *Many-Particle Physics*. Physics of Solids and Liquids. Springer US, 3 edition, 2000. ISBN 978-0-306-46338-9. URL <https://www.springer.com/gp/book/9780306463389>.

- [36] C. Roy and S. Hughes. Polaron master equation theory of the quantum-dot Mollow triplet in a semiconductor cavity-QED system. *Physical Review B*, 85(11):115309, March 2012. doi: 10.1103/PhysRevB.85.115309. URL <https://link.aps.org/doi/10.1103/PhysRevB.85.115309>.
- [37] Kaushik Roy-Choudhury and Stephen Hughes. Quantum theory of the emission spectrum from quantum dots coupled to structured photonic reservoirs and acoustic phonons. *Physical Review B*, 92(20):205406, November 2015. doi: 10.1103/PhysRevB.92.205406. URL <https://link.aps.org/doi/10.1103/PhysRevB.92.205406>.
- [38] C. Roy and S. Hughes. Influence of Electron–Acoustic-Phonon Scattering on Intensity Power Broadening in a Coherently Driven Quantum-Dot–Cavity System. *Physical Review X*, 1(2):021009, November 2011. doi: 10.1103/PhysRevX.1.021009. URL <https://link.aps.org/doi/10.1103/PhysRevX.1.021009>.
- [39] Dara P. S. McCutcheon and Ahsan Nazir. Quantum dot Rabi rotations beyond the weak exciton–phonon coupling regime. *New Journal of Physics*, 12(11):113042, November 2010. ISSN 1367-2630. doi: 10.1088/1367-2630/12/11/113042. URL <https://doi.org/10.1088/1367-2630/12/11/113042>.
- [40] T. Calarco, A. Datta, P. Fedichev, E. Pazy, and P. Zoller. Spin-based all-optical quantum computation with quantum dots: Understanding and suppressing decoherence. *Physical Review A*, 68(1):012310, July 2003. doi: 10.1103/PhysRevA.68.012310. URL <https://link.aps.org/doi/10.1103/PhysRevA.68.012310>.
- [41] Ahsan Nazir. Photon statistics from a resonantly driven quantum dot. *Physical Review B*, 78(15):153309, October 2008. doi: 10.1103/PhysRevB.78.153309. URL <https://link.aps.org/doi/10.1103/PhysRevB.78.153309>.
- [42] Aaron M. Jones, Hongyi Yu, John R. Schaibley, Jiaqiang Yan, David G. Mandrus, Takashi Taniguchi, Kenji Watanabe, Hanan Dery, Wang Yao, and Xiaodong Xu. Excitonic luminescence upconversion in a two-dimensional semiconductor. *Nature Physics*, 12(4):323–327, April 2016. ISSN 1745-2481. doi: 10.1038/nphys3604. URL <https://www.nature.com/articles/nphys3604>.
- [43] Lukas Chrostowski and Michael Hochberg. Silicon Photonics Design by Lukas Chrostowski, March 2015. URL [/core/books/silicon-photonics-design/BF3CF13E8542BCE67FD2BBC7104ECEAB](https://www.nature.com/core/books/silicon-photonics-design/BF3CF13E8542BCE67FD2BBC7104ECEAB).
- [44] Alexey Chernikov, Timothy C. Berkelbach, Heather M. Hill, Albert Rigosi, Yilei Li, Ozgur Burak Aslan, David R. Reichman, Mark S. Hybertsen, and Tony F. Heinz. Exciton Binding Energy and Nonhydrogenic Rydberg Series in Monolayer WS_2 . *Physical Review Letters*, 113

- (7):076802, August 2014. doi: 10.1103/PhysRevLett.113.076802. URL <https://link.aps.org/doi/10.1103/PhysRevLett.113.076802>.
- [45] Philippe K. Chow, Robin B. Jacobs-Gedrim, Jian Gao, Toh-Ming Lu, Bin Yu, Humberto Terrones, and Nikhil Koratkar. Defect-Induced Photoluminescence in Monolayer Semiconducting Transition Metal Dichalcogenides. *ACS Nano*, 9(2):1520–1527, February 2015. ISSN 1936-0851. doi: 10.1021/nm5073495. URL <https://doi.org/10.1021/nm5073495>.
- [46] Meinrad Sidler, Patrick Back, Ovidiu Cotlet, Ajit Srivastava, Thomas Fink, Martin Kroner, Eugene Demler, and Atac Imamoglu. Fermi polaron-polaritons in charge-tunable atomically thin semiconductors. *Nature Physics*, 13(3):255–261, March 2017. ISSN 1745-2481. doi: 10.1038/nphys3949. URL <https://www.nature.com/articles/nphys3949>.
- [47] S. Dufferwiel, S. Schwarz, F. Withers, A. a. P. Trichet, F. Li, M. Sich, O. Del Pozo-Zamudio, C. Clark, A. Nalitov, D. D. Solnyshkov, G. Malpuech, K. S. Novoselov, J. M. Smith, M. S. Skolnick, D. N. Krizhanovskii, and A. I. Tartakovskii. Exciton-polaritons in van der Waals heterostructures embedded in tunable microcavities. *Nature Communications*, 6(1): 1–7, October 2015. ISSN 2041-1723. doi: 10.1038/ncomms9579. URL <https://www.nature.com/articles/ncomms9579>.
- [48] V. Kravtsov, E. Khestanova, F. A. Benimetskiy, T. Ivanova, A. K. Samusev, I. S. Sinev, D. Pidgayko, A. M. Mozharov, I. S. Mukhin, M. S. Lozhkin, Y. V. Kapitonov, A. S. Brichkin, V. D. Kulakovskii, I. A. Shelykh, A. I. Tartakovskii, P. M. Walker, M. S. Skolnick, D. N. Krizhanovskii, and I. V. Iorsh. Nonlinear polaritons in monolayer semiconductor coupled to optical bound states in the continuum. *arXiv:1905.13505 [cond-mat, physics:physics]*, October 2019. URL <http://arxiv.org/abs/1905.13505>. arXiv: 1905.13505.
- [49] Xiaoze Liu, Wei Bao, Quanwei Li, Chad Ropp, Yuan Wang, and Xiang Zhang. Control of Coherently Coupled Exciton Polaritons in Monolayer Tungsten Disulphide. *Physical Review Letters*, 119(2):027403, July 2017. doi: 10.1103/PhysRevLett.119.027403. URL <https://link.aps.org/doi/10.1103/PhysRevLett.119.027403>.
- [50] F. Lohof, A. Steinhoff, M. Florian, M. Lorke, D. Erben, F. Jahnke, and C. Gies. Prospects and Limitations of Transition Metal Dichalcogenide Laser Gain Materials. *Nano Letters*, 19(1):210–217, January 2019. ISSN 1530-6984. doi: 10.1021/acs.nanolett.8b03729. URL <https://doi.org/10.1021/acs.nanolett.8b03729>.
- [51] C. Roy and S. Hughes. Phonon-Dressed Mollow Triplet in the Regime of Cavity Quantum Electrodynamics: Excitation-Induced Dephasing and Nonperturbative Cavity Feeding Effects. *Physical Review Letters*, 106(24): 247403, June 2011. doi: 10.1103/PhysRevLett.106.247403. URL <https://link.aps.org/doi/10.1103/PhysRevLett.106.247403>.

- [52] Ross Manson, Kaushik Roy-Choudhury, and Stephen Hughes. Polaron master equation theory of pulse-driven phonon-assisted population inversion and single-photon emission from quantum-dot excitons. *Physical Review B*, 93(15):155423, April 2016. doi: 10.1103/PhysRevB.93.155423. URL <https://link.aps.org/doi/10.1103/PhysRevB.93.155423>.
- [53] G. S. Agarwal. Additional vacuum-field Rabi splittings in cavity QED. *Physical Review A*, 43(5):2595–2598, March 1991. doi: 10.1103/PhysRevA.43.2595. URL <https://link.aps.org/doi/10.1103/PhysRevA.43.2595>.
- [54] H. J. Carmichael. Classical interpretation of “Additional vacuum-field Rabi splittings in cavity QED”. *Physical Review A*, 44(7):4751–4752, October 1991. doi: 10.1103/PhysRevA.44.4751. URL <https://link.aps.org/doi/10.1103/PhysRevA.44.4751>.
- [55] L. Tian and H. J. Carmichael. Incoherent excitation of the Jaynes-Cummings system. *Quantum Optics: Journal of the European Optical Society Part B*, 4(2):131–144, April 1992. ISSN 0954-8998. doi: 10.1088/0954-8998/4/2/007. URL <https://doi.org/10.1088%2F0954-8998%2F4%2F2%2F007>.
- [56] S. Weiler, A. Ulhaq, S. M. Ulrich, D. Richter, M. Jetter, P. Michler, C. Roy, and S. Hughes. Phonon-assisted incoherent excitation of a quantum dot and its emission properties. *Physical Review B*, 86(24):241304, December 2012. doi: 10.1103/PhysRevB.86.241304. URL <https://link.aps.org/doi/10.1103/PhysRevB.86.241304>.
- [57] Zhipeng Li, Tianmeng Wang, Zhengguang Lu, Chenhao Jin, Yanwen Chen, Yuze Meng, Zhen Lian, Takashi Taniguchi, Kenji Watanabe, Shengbai Zhang, Dmitry Smirnov, and Su-Fei Shi. Revealing the biexciton and trion-exciton complexes in BN encapsulated WSe₂. *Nature Communications*, 9(1):3719, December 2018. ISSN 2041-1723. doi: 10.1038/s41467-018-05863-5. URL <http://www.nature.com/articles/s41467-018-05863-5>.
- [58] P. Dey, J. Paul, Z. Wang, C. E. Stevens, C. Liu, A. H. Romero, J. Shan, D. J. Hilton, and D. Karaiskaj. Optical Coherence in Atomic-Monolayer Transition-Metal Dichalcogenides Limited by Electron-Phonon Interactions. *Physical Review Letters*, 116(12):127402, March 2016. doi: 10.1103/PhysRevLett.116.127402. URL <https://link.aps.org/doi/10.1103/PhysRevLett.116.127402>.
- [59] Jiao Xue, Ka-Di Zhu, and Hang Zheng. Detuning effect in quantum dynamics of a strongly coupled single quantum dot-cavity system. *Journal of Physics: Condensed Matter*, 20(32):325209, July 2008. ISSN 0953-8984. doi: 10.1088/0953-8984/20/32/325209. URL <https://doi.org/10.1088%2F0953-8984%2F20%2F32%2F325209>.

- [60] Robert Schmidt, Iris Niehues, Robert Schneider, Matthias Drüppel, Thorsten Deilmann, Michael Rohlfing, Steffen Michaelis de Vasconcellos, Andres Castellanos-Gomez, and Rudolf Bratschitsch. Reversible uniaxial strain tuning in atomically thin WSe₂. *2D Materials*, 3(2):021011, June 2016. ISSN 2053-1583. doi: 10.1088/2053-1583/3/2/021011. URL <https://doi.org/10.1088/2053-1583/3/2/021011>.
- [61] M. K. Agarwal and P. A. Wani. Growth conditions and crystal structure parameters of layer compounds in the series Mo_{1-x}W_xSe₂. *Materials Research Bulletin*, 14(6):825–830, June 1979. ISSN 0025-5408. doi: 10.1016/0025-5408(79)90144-2. URL <http://www.sciencedirect.com/science/article/pii/0025540879901442>.
- [62] Zhenghe Jin, Xiaodong Li, Jeffrey T. Mullen, and Ki Wook Kim. Intrinsic transport properties of electrons and holes in monolayer transition-metal dichalcogenides. *Physical Review B*, 90(4):045422, July 2014. doi: 10.1103/PhysRevB.90.045422. URL <https://link.aps.org/doi/10.1103/PhysRevB.90.045422>.
- [63] J.R. Johansson, P.D. Nation, and Franco Nori. QuTiP: An open-source Python framework for the dynamics of open quantum systems. *Computer Physics Communications*, 183(8):1760–1772, August 2012. ISSN 00104655. doi: 10.1016/j.cpc.2012.02.021. URL <https://linkinghub.elsevier.com/retrieve/pii/S0010465512000835>.
- [64] J.R. Johansson, P.D. Nation, and Franco Nori. QuTiP 2: A Python framework for the dynamics of open quantum systems. *Computer Physics Communications*, 184(4):1234–1240, April 2013. ISSN 00104655. doi: 10.1016/j.cpc.2012.11.019. URL <https://linkinghub.elsevier.com/retrieve/pii/S0010465512003955>.
- [65] A. Verger, C. Ciuti, and I. Carusotto. Polariton quantum blockade in a photonic dot. *Physical Review B*, 73(19):193306, May 2006. doi: 10.1103/PhysRevB.73.193306. URL <https://link.aps.org/doi/10.1103/PhysRevB.73.193306>.
- [66] Guillermo Muñoz-Matutano, Andrew Wood, Mattias Johansson, Xavier Vidal, Ben Q. Baragiola, Andreas Reinhard, Aristide Lemaître, Jacqueline Bloch, Alberto Amo, Gilles Nogues, Benjamin Besga, Maxime Richard, and Thomas Volz. Emergence of quantum correlations from interacting fibre-cavity polaritons. *Nature Materials*, 18(3):213–218, March 2019. ISSN 1476-4660. doi: 10.1038/s41563-019-0281-z. URL <https://www.nature.com/articles/s41563-019-0281-z>.